Use of silicon or carbonitriding interface in the adhesion of Ag-DLC film on titanium alloy: a comparative study

http://dx.doi.org/10.1590/0370-44672024770004

Adriano de Oliveira[1,5]
https://orcid.org/0009-0001-8655-296X
Argemiro S. da Silva Sobrinho[2,6]
https://orcid.org/0000-0001-7227-9176
Douglas M. G. Leite[2,7]
https://orcid.org/0000-0002-1792-6171
Jonas J. Neto[3,8]
https://orcid.org/0000-0002-8119-5932
Rodolfo L. P. Gonçalves[4,9]
https://orcid.org/0000-0001-5183-4636
Marcos Massi[4,10]
https://orcid.org/0000-0002-7117-8039

[1]Universidade Federal de São Paulo - UNIFESP,
São José dos Campos - São Paulo - Brasil.

[2]Instituto Tecnológico de Aeronáutica - ITA/DCTA,
Laboratório de Plasmas e Processos - LPP,
São José dos Campos - São Paulo - Brasil.

[3]Instituto de Estudos Avançados – IEAv/DCTA,
São José dos Campos - São Paulo - Brasil.

[4]Universidade Presbiteriana Mackenzie,
Escola de Engenharia,
São Paulo - São Paulo - Brasil.

E-mails: [5]adripampeano@gmail.com,
[6]argemiro@ita.br, [7]leite@ita.br, [8]jonas.jakutis@gp.ita.br,
[9]rodolfo.luiz99@gmail.com,
[10]marcos.massi@mackenzie.br

Abstract

A Hollow Cathode Plasma Enhanced Chemical Vapor Deposition (HC-PECVD) reactor was used to deposit silver doped Diamond-Like Carbon (Ag-DLC) films on Ti6Al4V alloy employing two methodologies: i) producing a silicon interlayer, using tetramethylsilane (TMS) as silicon precursor, varying the argon flow of the hollow cathode; and ii) carbonitriding the substrate. Profilometry, Raman, and Secondary Ion Mass Spectrometry (SIMS), as well as nanohardness, micro-scratch, scratch, and VDI 3198 indentation tests were used to evaluate the characteristics of the films and their adhesion on the substrates. The results demonstrated that the argon flow can be used for tuning the Ag-DLC film's hardness, toughness, and adherence on silicon interlayers. The carbonitriding process, in turn, provided an improvement in the film toughness compared with non-carbonitrided samples. Considering the lower cost and easier handling of N_2 compared to the silicon precursors commonly available (TMS, HDMSO, SiH_4, etc.), the carbonitriding process proved more appropriate to improve the adhesion of the Ag-DLC films on the Ti6Al4V alloy.

Keywords: diamond-like carbon, PECVD, hollow cathode, carbonitriding, titanium, scratch.

1. Introduction

Hydrogenated amorphous carbon (a-C:H) thin films are largely used as functional coating in biomedical applications where the wear strength is a requirement (Cemin *et al*., 2014; Meškinis & Tamulevičienė, 2011; Bonetti *et al*., 2006; Hauert *et al*., 2013). However, when the substrate is a metallic alloy, the film/substrate adherence becomes impaired due to the high compressive stress generated during the ion bombardment on the surface and the difference between the thermal expansion coefficients of both materials (Cemin *et al*., 2014; Bonetti *et al*., 2006; Chehung & Chien-Hung, 2008). Such different properties often result in delamination or peeling of the film and the consequent ion release from the interlayer or substrate to the organic environment. In the long term, this situation can result in toxic effects and allergic reactions (Singh *et al*., 2009; Gajski *et al*., 2014; De Morais *et al*., 2009; Oliver *et al*., 2019; Balachandran *et al*., 2020), requiring use of interlayers, which withstand the stress field generated by ion bombardment and increase the film toughness (Cemin *et al*., 2014; Bonetti *et al*., 2006).

Nanometric metallic interlayers containing Al, Cr, or Si are commonly used in this way with the metal precursors in liquid or gaseous phases (Cemin *et al*., 2014; Meškinis & Tamulevičienė, 2011; Liu *et al*., 2004). For substrates composed of titanium alloys, the silicon interlayers are the most widely employed, presenting excellent performance (Cemin *et al*., 2014; Bonetti *et al*., 2006). Although DLC films employed in environments where they are subject to chemical attacks by body fluids or friction during the use, the film can be damaged, exposing the silicon interlayer. Often, this exposition can result in a severe risk of stress corrosion cracking, due to the silicon/oxygen affinity and the high tribological loads that the interlayer is subjected to (Meškinis & Tamulevičienė, 2011; Hauert *et al*., 2013). Furthermore, according to Batory *et al*. (2015), when in contact with blood, the incorporation of silicon in the DLC film suppresses the formation of sp^2 graphitic clusters and promotes the hybridization of sp^3, which decreases the hemocompatibility of the film and can lead to the thrombosis. This result was also confirmed by Choi *et al*. (2008), who found that decreasing the sp^2/sp^3 ratio reduced the hemocompatibility and increased the hydrophilicity of DLC films. According to some studies (Sayes *et al*., 2007; Chen & Von, 2005; Valko *et al*., 2006; Kaewamatawong *et al*., 2006; Lin *et al*., 2006), the release of SiO_2 to the organism can also induce inflammatory and oxidative stress response and lead to cell damage. Furthermore, most of the liquid and gaseous silicon precursors are highly flammable and hazardous, requiring additional care during the handling.

To overcome the difficulties presented by use of silicon interlayers and its precursors, other alternatives are proposed to improve the film adherence, among them the use of a multilayer system (Bewilogua *et al*., 2011; Hainsworth & Uhure, 2013; Campoccia *et al*., 2013) with different functionalities, to grant composite-like characteristics to the surface. However, multilayer deposition is a complex process, sometimes demanding the use of several precursors and with a high risk of adhesive failure between the layers (Bewilogua *et al*., 2011, Campoccia *et al*., 2013). The use of thermochemical processes, such as nitriding and carbonitriding of the titanium surface for biomedical use, has been studied, but generally for direct contact with the organic tissues (Khandaker *et al*., 2016; Da Silva *et al*., 2011; Lin *et al*., 2011; Çaha *et al*., 2019; Ali *et al*., 2019). According to Khandaker *et al*. (2016) and Van Hove *et al*. (2015), the titanium surface nitriding promotes the surface bombardment with nitrogen ions and the consequent formation of Ti_2N and TiN_x ($0.43 < x < 1.08$) precipitates in the α-Ti matrix. Titanium nitrides are marked by their high biocompatibility and blood tolerability allied with high wear and fracture strength (Khandaker *et al*., 2016; Van Hove *et al*., 2015; She *et al*., 2015). On the other hand, thermochemical treatment of the titanium surface replacing the silicon interlayer has not gained attention.

In summary, DLC films for coating biomaterials have been studied ostensibly through various deposition techniques (Zia, A. W. & Birkett, M., 2021), however, the technique of PECVD operated with a hollow cathode, as a way of doping DLC films with Ag for use in biomaterials, is still little explored. Therefore, this study aims to evaluate the influence of a silicon interlayer compared to carbonitriding on the adhesion of Ag-doped DLC films on titanium alloys using a hollow cathode PECVD reactor. The study was conducted using two methodologies: i) using a silicon interlayer and ii) carbonitriding the titanium substrates. The characteristics of the films were evaluated by means of profilometry, Raman spectroscopy and secondary ion mass spectrometry (SIMS), as well as nano-hardness, micro-scratches, scratch tests and VDI 3198 (1991) standard indentation tests.

2. Experimental procedures

Titanium alloy disks (Ti6Al4V), with 10 mm diameter and 3 mm thickness, were used as substrates, which were prepared using 280 to 2,000 grit sandpaper and polished with 0.6 µm colloidal silica. After that, the deposition of DLC films and the carbonitriding processes were performed in a cylindrical hollow cathode PECVD reactor with 300 mm diameter and 450 mm height, using an EM18 Edwards vacuum pump. The main plasma in the substrate holder was generated by a pulsed DC Pinacle Plus 5 kW + 5 kW power supply from Advanced Energy. The sample temperature was monitored by a thermocouple installed at the bottom of the substrate holder. All the samples were doped with silver nanoparticles for trials to be performed in a later study. The hollow cathode plasma used to dope the DLC film with Ag was placed inside the reactor, near the substrate holder. An electric power of 60W was applied on a silver hollow cathode. An argon flow (99.99% purity) inside the hollow cathode carried the silver to the samples The dimensions of the hollow cathode are illustrated in Figure 1.

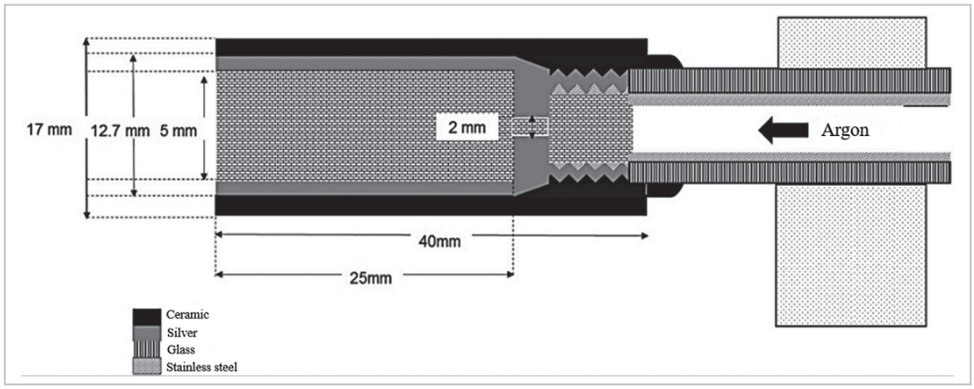

Figure 1 - Schematic representation of the hollow cathode showing its dimensions and materials that compose it.

On an AISI 300 stainless steel planar cathode (diameter: 100mm; thickness: 5mm) an electric voltage was applied (varied from 300V to 450V). This plasma system was used to deposit Ag-DLC films on Ti6Al4V using two kinds of interfaces: i) a silicon interlayer, using tetramethylsilane (TMS) as the silicon precursor, varying the argon flow of the hollow cathode and ii) carbonitriding the substrate.

A "ring shower" placed on the top of the chamber supplied methane (CH_4 - 99.99% purity) and/or N_2, used as carbon and nitrogen precursors, respectively. For a better evaluation of Ag-DLC film adherences, the samples were divided into two groups (Table 1), both containing carbonitrided and non-carbonitrided samples. In the first one (Group 1), in which the process times were smaller, the aim was to analyze the behavior of the DLC films subjected to low loads in the scratch test. Hence, the DLC film adherence was characterized by nanohardness and micro-scratch test. For the second group (Group 2), the process times were increased to obtain thicker films and analyze the behavior of the DLC films under greater loads in the scratch test.

The schematic diagram of the plasma system is in Figure 2.

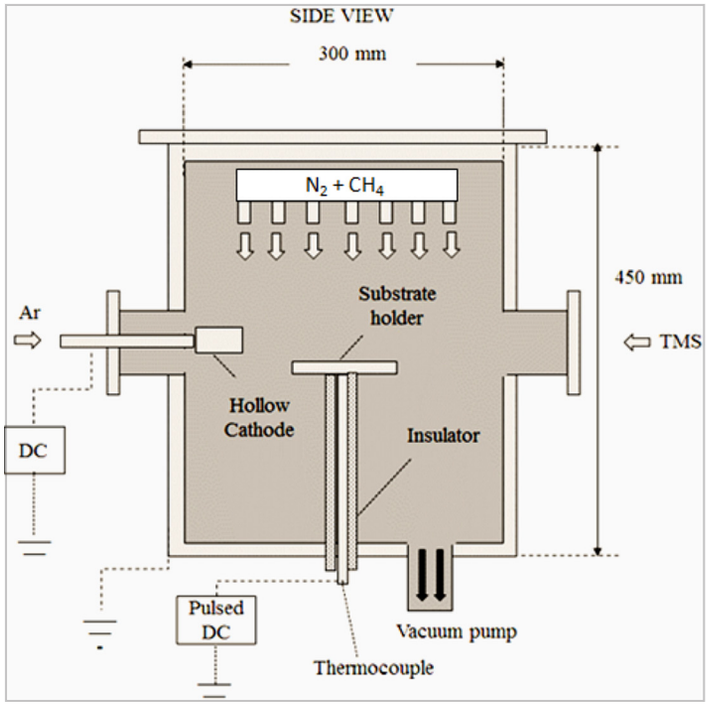

Figure 2 - Schematic diagram showing the main components of the hollow cathode PECVD reactor.

For both groups, the deposition processes followed the steps:

a) First it was heated to 530 °C and pressure of 3 Torr for carbonitriding (samples CN20-1, CN20-2, and CN20-3) and for silicon interlayer (samples Si20, Si60, Si80, and Si100), at different process times, see Table 1.

In the carbonitriding process, N_2 (80 sccm) and CH_4 (5 sccm) were used as nitrogen and carbon precursors, respectively. The silicon interlayers were grown using tetramethylsilane (TMS) as the silicon precursor.

b) The substrate was cooled from 530 °C to the Ag-DLC work temperature (approximately 150 °C);

c) Ag-DLC film were deposited at pressure of 0.4 Torr, using 5 sccm of methane as carbon precursor. For Group 1, the DLC deposition time was 15 min and for Group 2, 60 min. The argon flow was changed during the DLC film deposition for evaluation of its relationship with the film adherence to the substrate.

During the substrate cooling, the cooling rate of non-carbonitrided samples have always been higher than the cooling rate of that carbonitrided, the latter always resulting in thicker Ag-DLC films. This occurs because the thermal conductivity of the silicon interlayers (250 – 270 $W.m^{-1}.K^{-1}$) (Román-Manso *et al.*, 2016) is higher

than that of the carbonitrided layers (15 – 30 $W.m^{-1}. K^{-1}$) (Zhang, 1993).

For the first group of samples (Group 1), the following characterization methods were performed:

- Profilometry: to measure film thickness using a KLA Tencor P-7, with scan speed of 50 µm/s, acquisition rate of 200 Hz, load of 2 mg and resolution of 13 µm/0.0078Å. Si (100) wafers were used as witness samples.

- Raman Spectroscopy: Horiba Evolution, with a 600 lines/mm diffraction grid. The adopted procedure used three accumulations with an acquisition time of 30 s.

- Secondary Ion Mass Spectrometry: to determine the chemical composition depth profile using a SIMS Workstation from Hyden Analytical with a MAXIM Quadrupole for mass detection, working pressure of 10^{-8} Torr, resolution of 1/300 amu, argon ion gun, and removal capacity of 1 nm. The chemical analysis of the coating was performed using an Ar^+ ion beam with energy of 3 kV incident on the film surface.

- Nanohardness test: using an Anton Paar Micro-Scratch Tester (MST3) with a Berkovich diamond indenter. The acquisition rate was 10 Hz, approach distance of 3,000 nm, linear loading with an approach speed and retract speed of 16,000 nm/min, maximum load of 3 mN, loading rate of 6 mN/min, unloading rate of 6 mN/min, pause of 10 s, and stiffness threshold of 500 µN/µm. This characterization provided the film hardness in MPa. The room temperature was 25 °C and the relative humidity 53%.

- Micro-Scratch test: An Anton Paar Micro-Scratch Tester (MST3) with an HRC conic diamond indenter was used. The advance speed was 1 mm/min. The start load was 30 mN and the end load was of 10,000 mN, with a speed of 1 mm/min applied over 2 mm of distance. The ASTM C1624-05 (2015) Norm was adopted as a test procedure, with the following three stages of critical loads: Lc1 for crack starting, Lc2 for starting of substrate exposition, and Lc3 for full substrate exposition.

- Rockwell C hardness for Group 1 test: using a Wilson Durometer model 1JR with load of 150 kgf.

- Rockwell C hardness for Group 2 test: CETR Tribometer, model UMT with a Rockwell C diamond tip with radius of 200 µm, speed of 166 µm/s, acquisition time of 30 s, over 5 mm of distance. The load used was 20 N. Table 1 shows the process parameters of both groups.

Table 1 - PECVD process parameters for Groups 1 and 2.

Group	Sample	Treatment	Interlayer/Carbonitriding			DLC			
			Pressure (Torr)	Temperature (°C)	Time (min)	Pressure (Torr)	Power (W)	Time (min)	Argon flow
1	Si20	Silicon Interlayer	3	530	10	0.4	15	15	20
	Si80	Silicon Interlayer			10				80
	CN20-1	Carbonitriding			60				20
2	Si60	Silicon Interlayer	3	530	30	0.4	15	60	60
	Si100	Silicon Interlayer			30				100
	CN20-2	Carbonitrided			90				100
	CN20-3	Carbonitrided			90				100

3. Results and discussion

3.1 Analyses of Group 1

3.1.1 Profilometry

Figure 3 shows DLC film thicknesses of the Group 1 samples. The increase in the argon flow reduced the film thickness from around 0.8 µm to 0.25 µm. This result is related to the combined effect of argon and CH_4 flows of the DLC film deposition process, which involves not only reduction in the deposition rate, but also an increase in the etching rate promoted by argon atoms (Jones & Nelson, 2016; Kim & Lee, 2003).

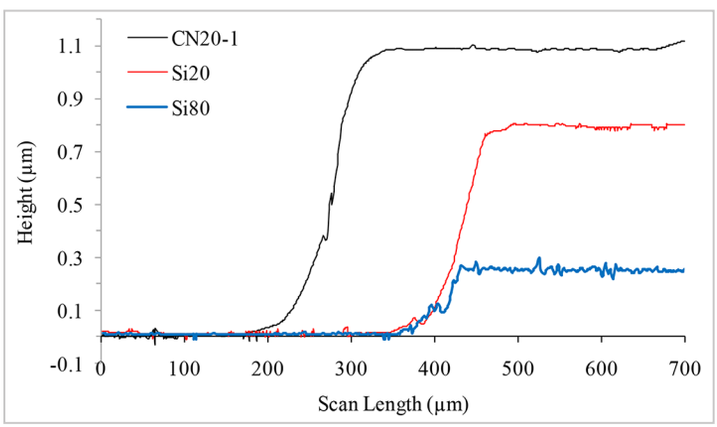

Figure 3 - Thickness profiles of DLC films of the Group 1 samples.

The effect of the etching process can also be seen by the profile curve obtained in the sample Si80, where the DLC film surface is rougher than the surface of the Si20 sample.

The carbonitrided sample CN20-1 in turn, presented the thickest DLC film among the samples, of around 1 µm, caused by the slow cooling rate of carbonitriding process in comparison with non-carbonitriding process. This is related to the higher thermal conductivity of the silicon interlayers compared with that of the carbonitrided layers, resulting in greater time with the plasma turned on during the cooling of the sample until the DLC film deposition temperature.

3.1.2 Raman spectroscopy

Raman spectra of the samples Si20 and Si80 presented D and G bands characteristic of DLC films, located between the wavelengths 1,350 cm^{-1} and 1,580 cm^{-1} (Figure 4). While the G band of the sample Si20 was located at 1,575 cm^{-1}, for sample Si80, in which the DLC film was grown with the higher argon flow, this band was located at 1,558 cm^{-1}, moving away from the crystalline graphite wavelength (1,580 cm^{-1}), showing an increase in the film amorphization (Robertson, 2002; Grenadyorov, 2018) due to the increased argon ions bombardment (Hauert, 2004).

The comparison of the FWHMG values of 122 cm^{-1} for sample Si20 and 140 cm^{-1} for sample Si80 also evidence this tendency. The D band of both samples did not present substantial changes.

The sample CN20-1 also presented D and G bands characteristic of DLC films, with D and G values located at 1,336 cm^{-1} and 1,545 cm^{-1}, respectively. The FWHMG of this sample was 157 cm^{-1}, which characterizes an amorphization degree larger than for both other samples, suggesting a DLC film with higher density and elevated hardness (Lima-Oliveira *et al.*, 2012). This result is related to the diffusion-barrier formed by carbonitriding process on the titanium surface, hampering the rapid diffusion of hydrogen and carbon into the substrate. This barrier promotes the formation of carbides and saturation of carbon on the titanium surface (Fu *et al.*, 2000).

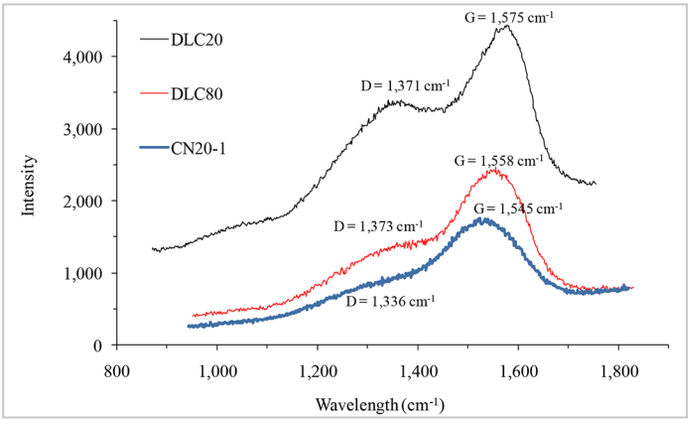

Figure 4 - Raman spectra of the samples Si20, Si80, and CN20-1.

3.1.3 Secondary ion mass spectrometry - SIMS

Figure 5 and Figure 6 show the chemical composition gradient of the main chemical elements in the Ag-DLC film of the CN20-1 sample. The goals of SIMS characterization were to evaluate the effectiveness of the carbonitriding process, by means of the nitrogen presence in the DLC/substrate interface, and also estimate the Ag-DLC film thickness. In both figures, the chemical analysis from Ag-DLC surface up to Ti substrate is plotted from left to right, showing a reduction of both nitrogen content (from 8,000 to 2,000 counts) and carbon (from 100,000 counts to very low values). These results indicated that the thickness of the film is around 1 µm, and this is the interface between the substrate and the DLC film. Although the N counts decreased near the substrate, its presence was still detected below.

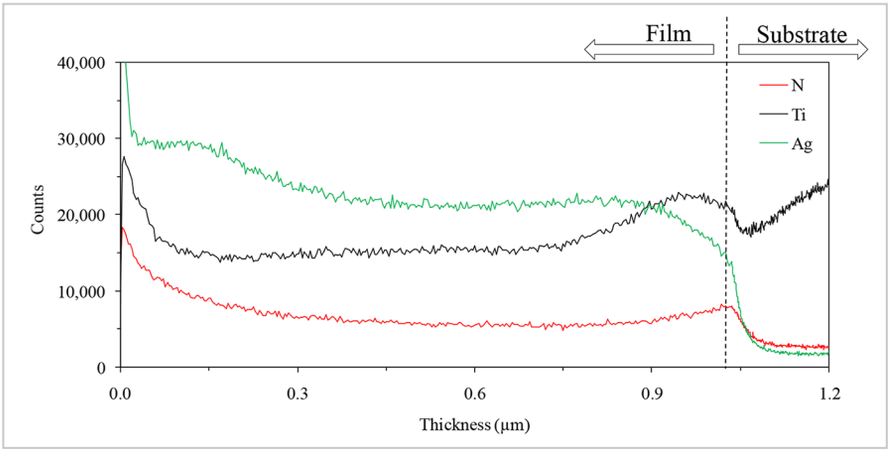

Figure 5 - SIMS curves showing N, Ti, and Ag gradients throughout the DLC film for sample CN20-1.

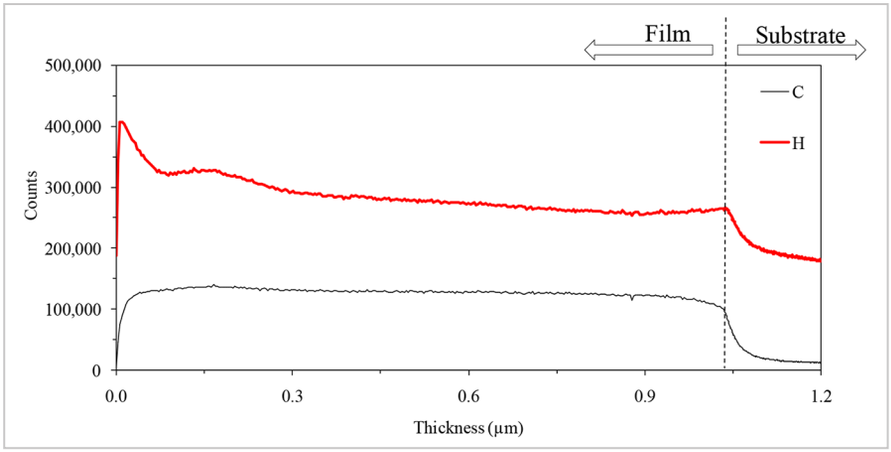

Figure 6 - SIMS curves indicating C and H gradients throughout the DLC film for sample CN20-1.

the Ti surface, confirming the carbonitriding of the sample. The low count of nitrogen in the substrate could be related to the higher ionization energy of this element and the stability of its formed compounds. Furthermore, Ti was detected throughout the film due the surface sputtering process during the deposition. From 1 µm below the DLC film surface, its count increased, confirming that the SIMS electron beam reached the titanium alloy surface. The increase of H and Ag on the film surface is related to the interruption of the argon flow in the last minute of the process, maintaining only the N_2 and CH_4 flowing through the silver hollow cathode. The aim of this procedure was to enrich the DLC film surface with silver, to improve further biological response. The high hydrogen count on the DLC film surface could also be related to the active role of titanium in the hydride formation, which may explain the quick increase of both elements near this region (Lima-Oliveira *et al.*, 2012; Fu *et al.*, 2003).

3.1.4 Nanohardness and micro-scratch tests

As can be seen in Figure 7, for samples with silicon interlayer (Si20 and Si80), the increase in argon flow (from 20 to 80 sccm) allowed a hardness of 10,440 MPa to be reached, an average increment of more than 2,000 MPa in relation to Si20 hardness.

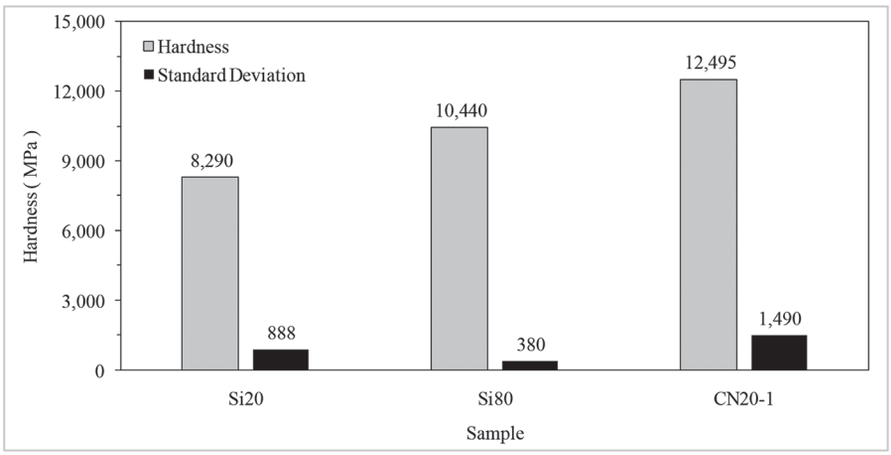

Figure 7 - Nanohardness for samples of Group 1.

If the substrates were a very hard material, at least some part of this increase could be because sample Si80 has an indentation depth (± 0.18 nm for all samples) greater than 20% of the film thickness and the substrate hardness would affect the measurement (Lin *et al.*, 2004). However, the Ti6Al4V alloy used in this study, has a low hardness of around 505 MPa. An increased FWHMG indicates the rise in the sp^3 hybridization, which characterizes films with best adherence and mechanical strength that are suitable for biomedical applications where the material is subject to load bearing and wear (Hellmich *et al.*, 1998; Koike *et al.*, 1992). Several studies found that the increase in the argon flow promotes the rise in the ion bombardment leading to the preferential removal of sp^2 sites due to its lower bonding energy (Bigerelle *et al.*, 2005; Lackner *et al.*, 2012; Chau-Chang *et al.*, 2013; Vetter, 2014). Robertson (1994; 2002) found that the carbon atoms implanted during the plasma deposition promotes a metastable increase of the film density and supports sp^3 bonding. Khettache *et al.* (2002) and Peng *et al.* (2001) also confirmed that a-C:H films grown with higher argon flows presented greater sp^3 bonding due to the diffusion barrier formed by ions embedded in the surface.

In the carbonitrided sample, the film hardness was even greater, reaching 12,495 MPa. Although Vandevelde *et al.* (1998) and Lin *et al.* (2004) associated the presence of nitrogen in the DLC film to a decrease in its hardness and quality, Bootkul *et al.*(2014) and Derradji *et al.*(2005) found that increasing the N content in the DLC film, induced changes in the arrangement of C sp^3 sites from graphitic to pyridine-like structures and nitrile bonds, which breaks the interconnection of the graphitic structure of the film and can induce some

increase in the hardness. Despite the great thickness of the DLC film in this sample, to a certain extent, its high hardness can also be affected by increased substrate tensile strength, due to the precipitation of very hard compounds, such as TiC_xN_y, Ti_2N, and TiN_x, on the alloy surface and by solid solution hardening of α-Ti matrix by nitrogen (Perry, 1981; Tamura *et al.*, 2002).

The micro-scratch test provides a quantitative engineering measurement of the practical adhesion strength and damage resistance of the coating-substrate system as a function of the applied normal force (ASTM C1624-05). The friction coefficients are presented in Figure 8 from the micro-scratch tests performed on the three samples of Group 1. While for sample Si20, the friction coefficient started at values lower than 0.05 and after 0.1 mm increased quickly to values over 0.4, for sample Si80, they were under 0.15 up to 1.8 mm, denoting upper adhesion strength. On the other hand, sample CN20-1 presented a different behavior according to the tip advance. The friction coefficient started in 0.15 and presented some peaks with values between 0.25 and 0.30 along the track, returning to 0.15 again. For a better understanding of the failure mechanisms, a detailed analysis was conducted comparing the critical loads (Lc), failure modes, and acoustic emission (AE) signals.

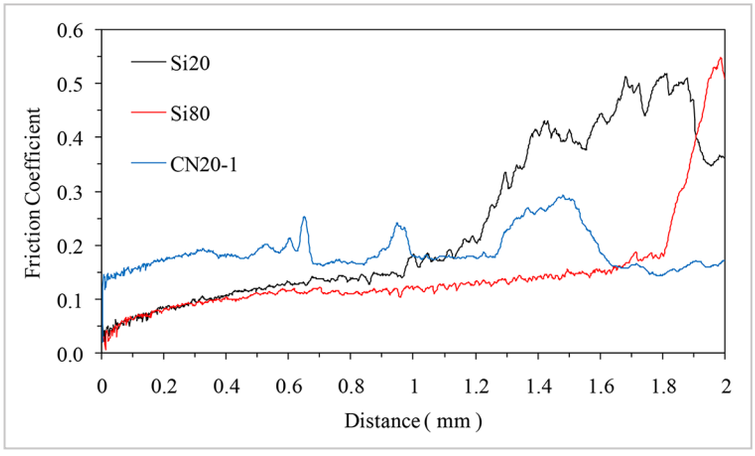

Figure 8 - Friction coefficient for samples Si20, Si80, and CN20-1.

Figure 9 shows the result of the micro-scratch test for sample Si20, and in the upper section, exhibits the image of the track generated by the indenter during the test. Right below, the friction coefficient along the track is presented, then the applied normal force (diagonal line) and the acoustic emission during the path. The bottom section illustrates the magnification of the areas where the critical loads occurred, indicated by dashed arrows. The horizontal black arrows indicate the

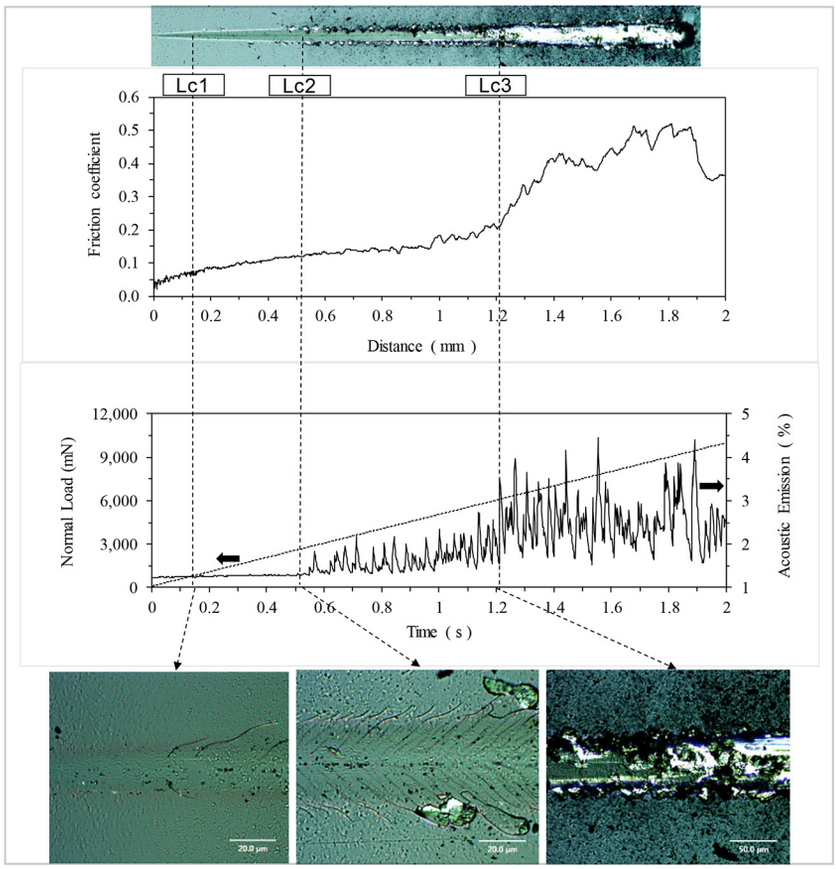

Figure 9 - Friction coefficient, acoustic emission and start point of critical loads of sample Si20.

vertical axis related to that curve. Using the average value of AE signal from sample Si20, it was possible to determine the place where the cracks started. The first Chevron cracks, cohesive failures with a "V" shape (Perry, 1981; ASTM C1624-05), occurred between 0.1 mm and 0.2 mm from the track beginning, with Lc1 = 900 mN. The AE signal was primal for the definition of Lc2. From 0.6 mm to 1.2 mm, this signal presented an average gain of 20%, increasing from 1.28% to 1.61%. This denotes that around 0.5 mm, the progressive load reached the critical value Lc2 = 2,900 mN and the film cracking is not sufficient to relieve the stress promoted by the indenter, signaling a region where the delamination (adhesive failure) was the main failure mode (Perry, 1981; ASTM C1624-05). After 1.2 mm, AE presented a new gain of 55%, increasing from 1.61% to 2.5%, denoting the full exposition of the film.

Figure 10 shows the result of the micro-scratch test for sample Si80 and exhibits the evolution of the same parameters presented in Figure 9. In this case, all the critical loads measured for sample Si80 are higher than those of the sample Si20, reaching the maximum value of Lc3 = 9,100 mN, while for Si20 the Lc3 remained at 6,100 mN (Figure 11). Another relevant result was the different amplitude of the AE signal for both samples. While the signal amplitude for Si20 was limited to 5%, for Si80, the AE signal exceeded 40% (Figure 10). According to Sekler *et al.* (1988) and Tomastik *et al.* (2018), the signal amplitude is proportional to the energy released by microcracks formed during the indenter pathway. Considering this result and the fact that the nanohardness of the sample Si80 DLC film presented a Young's Modulus of 10.4 GPa, while for the sample Si20, this value was 9.1 GPa, it is possible to state that the failure formation energy for sample Si80 was higher than for the Si20 sample. This could explain the amplitude difference of the AE signals and suggests an improvement in the cohesive strength of the Si80 DLC film, confirming the important role of the increased argon flow in the sp^3 bonding formation of this sample.

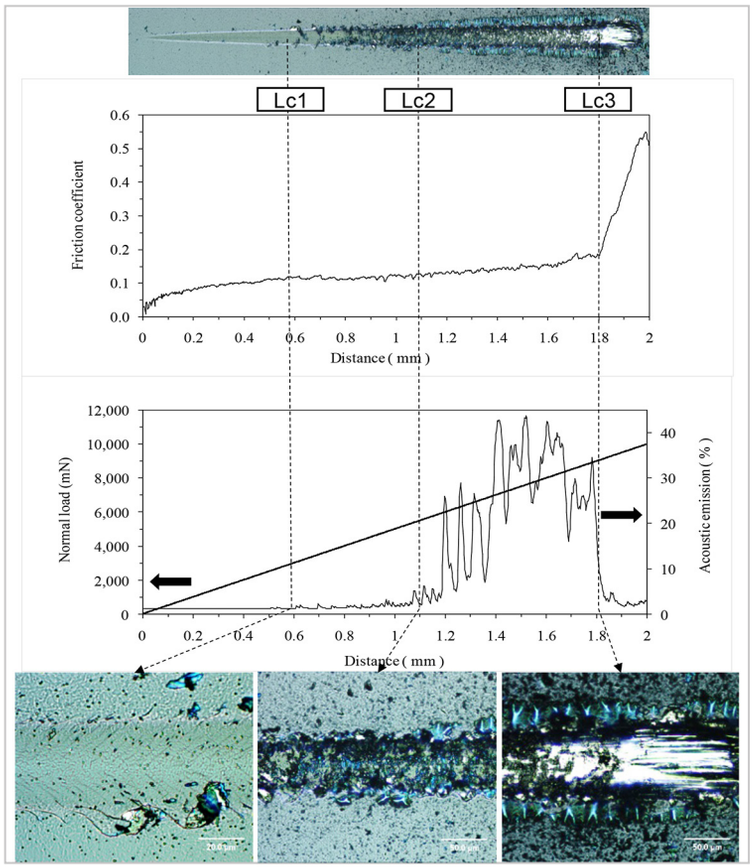

Figure 10 - Friction coefficient, acoustic emission, and start point for critical loads of sample Si80.

The borders of the scratch tracks of both samples also presented some outstanding differences in the failure modes (Figure 12). This can be seen in the areas bounded by dashed lines for samples Si20 and Si80, in the track borders after 1 mm of the scratch track starting. While in the sample Si20, the failures were characterized by film detachment in this region, in sample Si80, the film buckling was the prevalent failure mode. This result suggests that although the increased argon flow promoted a decreased sp^2/sp^3 ratio, it also promoted the increased Young's Modulus and enabled the deposition of a more ductile film, which was able to withstand the buckling promoted by the indenter without breaks and resulted in best adherence (Bull & Berasetegui, 2006; Burnett & Rickerby, 1988). For the toughness of the DLC films, some researchers have used only the lower critical load (Lc1) to indicate the "crack toughness" of the films (Pei *et al.*, 2005; Shum *et al.*, 2004; Ligot *et al.*, 2000), while others (Yonghui & Xiang, 2015; Zhang & Zhang, 2012; Zhang *et al.*, 2005) have pointed out that this parameter should be proportional to both, the lower critical load (Lc1) and the difference between the load where the film starts to peel (Lc2) and the lower (Lc1) critical load. Obviously, a film can have an early crack, but if it fractures or peels off at very high load, the film has a very high "toughness" because, during the measurement, the coating successfully resisted the propagation of the crack, so

it is very reasonable that Lc2 should be considered in the film toughness measurement. This quantitative calculus of the film toughness suggested by Zhang & Zhang (2012) was performed by using the following equation:

$$CPR = Lc1*\{K*(Lc2-Lc1)\}$$

where: - CPR is the Crack Propagation Resistance; - K is a correction coefficient related to the film properties.

Applying this formula to both DLC films of samples Si20 and Si80, the following results were obtained:

$$CPR\ Si_{20} = 1.80 \times 106.K$$

$$CPR\ Si_{80} = 2.55 \times 106.K$$

The ratio between CPR Si_{80} and CPR Si_{20} results in a 41% increase in the CPR, evidencing the high effectiveness of the increased argon flow on the toughness of the DLC film.

Figure 11 shows a comparison of the critical loads of the three Group 1 samples.

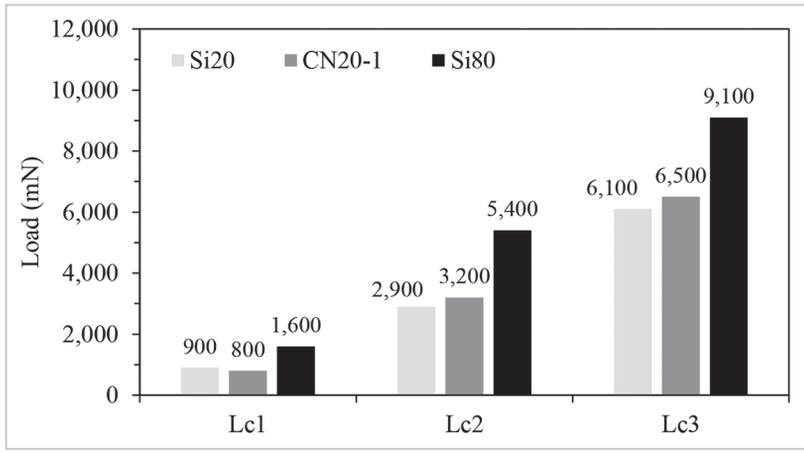

Figure 11 - Critical loads for samples Si20, Si80, and CN20-1.

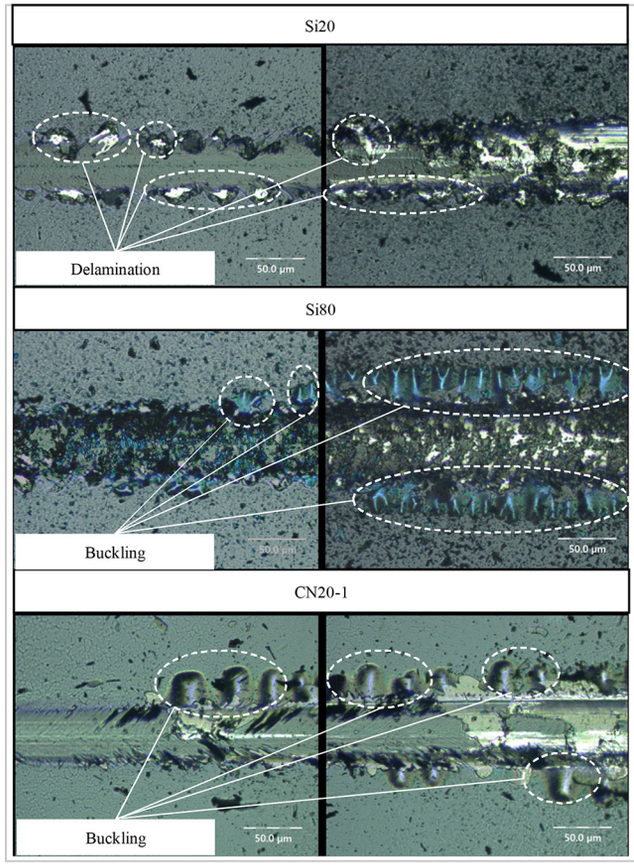

Figure 12 - Failure modes in the track borders after 1 mm of the scratch track starting: sample Si20 (delamination), Si80 (buckling), and CN20-1 (buckling).

In the micro-scratch test of sample CN20-1 (Figure 13), the values of Lc1 and Lc2 remained near those obtained for sample Si20 (Figure 11). Even with the absence of a silicon interlayer, the friction coefficient of CN20-1 was 0.15 in the beginning of the test remained under 0.2 up to 0.6 mm. Between 0.6 mm and 1.3 mm, the friction coefficient presented oscillations with high peaks that returned to the lower level, which according to Perry (1981) characterize carbonitrided surfaces. Considering the purposed biomedical use of this film, for many applications a very low friction coefficient is not interesting or necessary because in general, it means a hydrophilic surface, which can thwart the cellular adhesion (Campoccia *et al*., 2013; Caravaca, 2016; Liu *et al*., 2004; Vasudev *et al*., 2013). On the other hand, sample CN20-1 presented substantial adhesion strength along the micro-scratch track, with greater Lc2 and Lc3 values than the Si20 sample (Figure 11). The improvement in the adhesion strength of sample CN20-1 compared with the sample Si20 is also characterized by the failure mode in the track border at the 1 mm position of the micro-scratch test (Figure 12), where the film withstood the buckling promoted by the indenter without breaks resulting in high adherence (Bull & Berasetegui, 2006; Burnett & Rickerby, 1988). The choice of the position at 0.9 mm for Lc2 critical load occurrence, and not some point between 0.5 mm and 0.7 mm, was based on the procedure defined in the ASTM C1624-05, which establishes that any critical load should be associated with the occurrence of the same failure in both sides of the track. Quantitatively, the CPR value for sample CN20-1 was 1.92 × 106.K, achieving a 6.6% increase in the crack toughness for the Si20 sample.

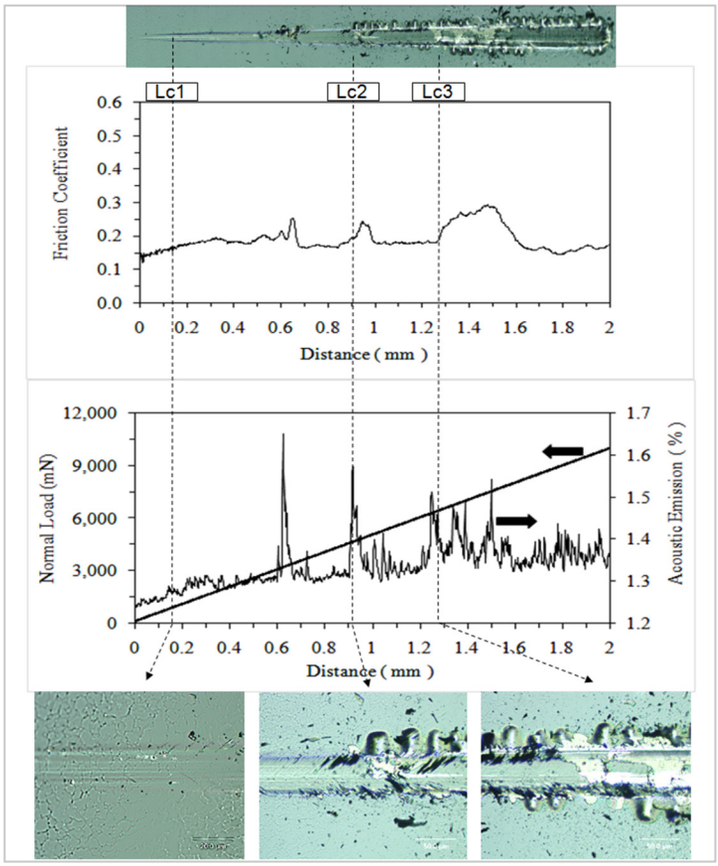

Figure 13 - Friction coefficient, acoustic emission, and start point of critical loads for sample CN20-1.

3.1.5 VDI 3198 indentation test

The VDI 3198 indentation test is a fast characterization method for film adherence (Lugo *et al*., 2017; Capote *et al*., 2018; Standard VDI 3198, 1991). The test uses a conical indenter to penetrate a diamond indenter into a coating surface, causing extensive plastic deformation of the substrate and fracture of the coating. Figure 14 is the SEM images of the indentation areas at 45° slope for Group 1 samples. Table 2 provides the EDX chemical analysis of both the DLC films (Area 1) and the delaminated area (Area 2), after VDI 3198 indentation test for each sample. As can be seen, sample Si20 presented extensive delamination of the DLC film and silicon interlayer, fully exposing the titanium substrate (Figure 14), which can be confirmed by the high amount of Ti (73.8 wt%) and Al (9 wt%) detected in Area 2. For Sample Si80, the DLC film delaminated, while silicon interlayer remaining adhered to the substrate. In this case, Area 2 presented Ti and Al amounts of 9.9 wt% and 2.2 wt%, respectively. The amount of Si and O were 13 wt% and 5.4 wt%, respectively, denoting characteristics of the silicon interlayer.

Unlike sample Si20, at the borders of the delaminated area of sample Si80, little parts of the film (white dashed lines) are visible, which bended without breaking, demonstrating a slight improvement in the film toughness. In the case of sample CN20-1, the delaminated region (Area 2) presented elevated amounts of Ti and Al, but not as high as sample Si20. Considering that the carbon amount in this area was 10.5 wt%, this result suggests the presence of compounds with high stability like carbonitrides (Ti_2N and TiN_x), as mentioned by Khandaker *et al*. (2016) and Van Hove *et al*. (2015). This

sample also presented a peculiar aspect around the imprint border, where it is possible to see areas (white dashed lines) in which the film bent without breaking, evidencing a pronounced improvement in the film toughness.

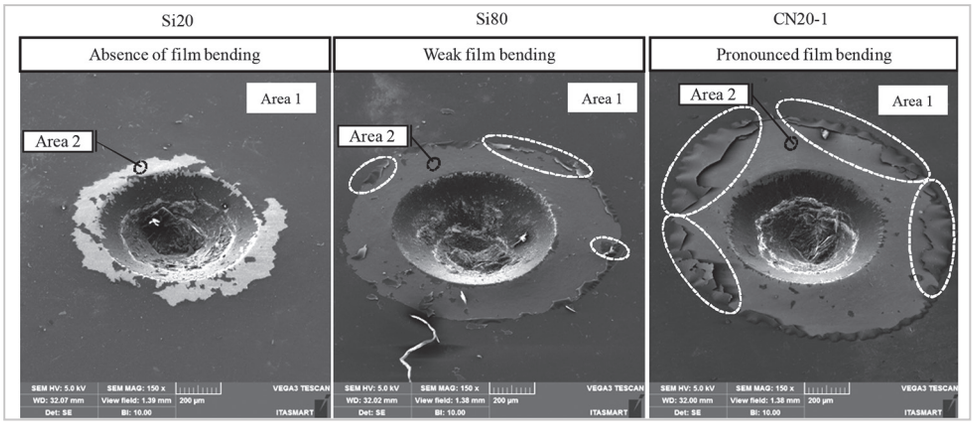

Figure 14 - Comparison of film bending around HRC indenter imprint for samples Si20, Si80, and CN20-1 (SEM - 45° slope - 150x).

Table 2 - SEM chemical analysis of DLC film and delaminated area for Group 1 samples.

Sample	Area 1 (%wt.)					Area 2 (%wt.)				
	C	Si	Ti	O	Al	C	Si	Ti	O	Al
Si20	77.8	7.9	7.3	5.6	0.9	73.8	0.2	73.8	2.7	9.0
Si80	77.4	10.4	6.7	3.8	0.8	69.4	13.0	9.9	5.4	1.2
CN20-1	75.0	0.2	21.5	-	2.5	10.5	0.4	67.0	11.0	8.0

3.2 Group 2

3.2.1 Profilometry

Figure 15 shows the profilometry characterization of the Group 2 samples. Both Si60 and Si100 presented a thickness of around 5 µm, although the last one had a rougher surface owing to the increase in the ion bombardment caused by higher argon flow in this process deposition. Samples CN20-2 and CN20-3, in turn, presented DLC film thicknesses of 8.8 µm and 8.3 µm, respectively, the highest values among all the DLC films. This result is related to the greater time needed to cool the substrate from 530 to 150 °C, in which the plasma is turned on. In general, these films are smoother than those without the carbonitrided layer. According to Luo (2009), for hard films deposited by plasma, increasing the thickness trends to generate a smoother film surface due the low influence of the substrate roughness and the extended time that the indenter remains sliding on the film.

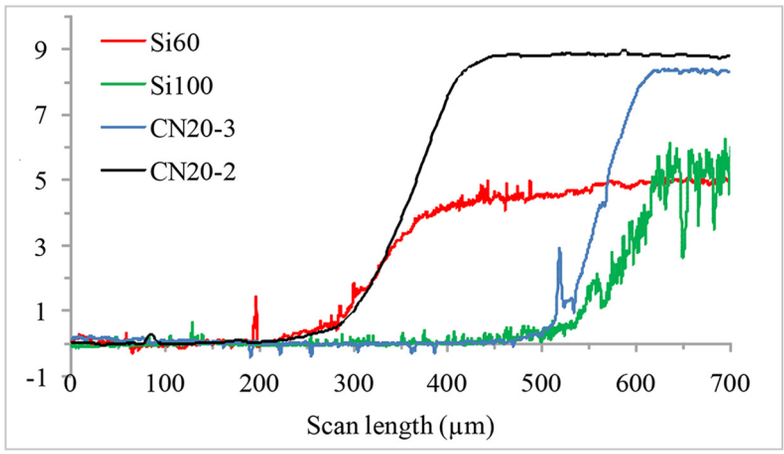

Figure 15 - DLC film thicknesses for Group 2 samples.

3.2.2 Scratch-test

Figure 16 shows the scratch tests performed on Group 2. The upper and central regions of this figure present the friction coefficients of both non-carbonitrided (Si60 and Si100) and carbonitrided (CN20-2 and CN20-3) samples, while the lower region presents the normal force used in the tests.

The non-carbonitrided samples (Si60 and Si100), maintained their friction coefficients under 0.15 up to 3.2 mm, even with a load of 20 N, which is higher than

that used for non-carbonitrided samples in Group 1 (Si20 and Si80). This behavior is related to the promotion of the sp3 hybridization due to the increased argon flow, which characterizes films with best mechanical strength (Hellmich *et al*., 1998; Steffen *et al*., 1992; Koike *et al*., 1992).

However, beyond the influence of the argon flow, the increase of the film thickness from Group 1 to Group 2 also seems to have influenced the holding of the friction coefficient at low values when comparing samples Si60 (Group 2) with Si80 (Group 1), for example. Ma *et al*. (2003) observed the dependence of tribological properties of DLC films related to its thickness. Sheeja *et al*. (2002), Qi *et al*. (2001), and Luo (2009) observed that for hard films, the friction coefficient decreases with the increasing of its thickness, due the low influence of the substrate roughness and the extended time that the indenter keeps sliding on the film. Despite the better performance of the Group 2 non-carbonitrided, samples compared to the Group 1 samples, their performance did not surpass those obtained for Group 2 carbonitrided samples (CN20-2 and CN20-3). This result can be seen at least up to 4.5 mm, where the DLC film from sample CN20-2 presented a failure and its friction coefficient grew abruptly. This failure can be related to some film imperfection or surface contamination, because the DLC film of sample CN20-3, grown with the same conditions, maintained its friction coefficient under 0.15 up to the end of the test, withstanding a normal force up to 15 N, which is 50% above the maximum load (10 N) employed in the CN20-1 sample.

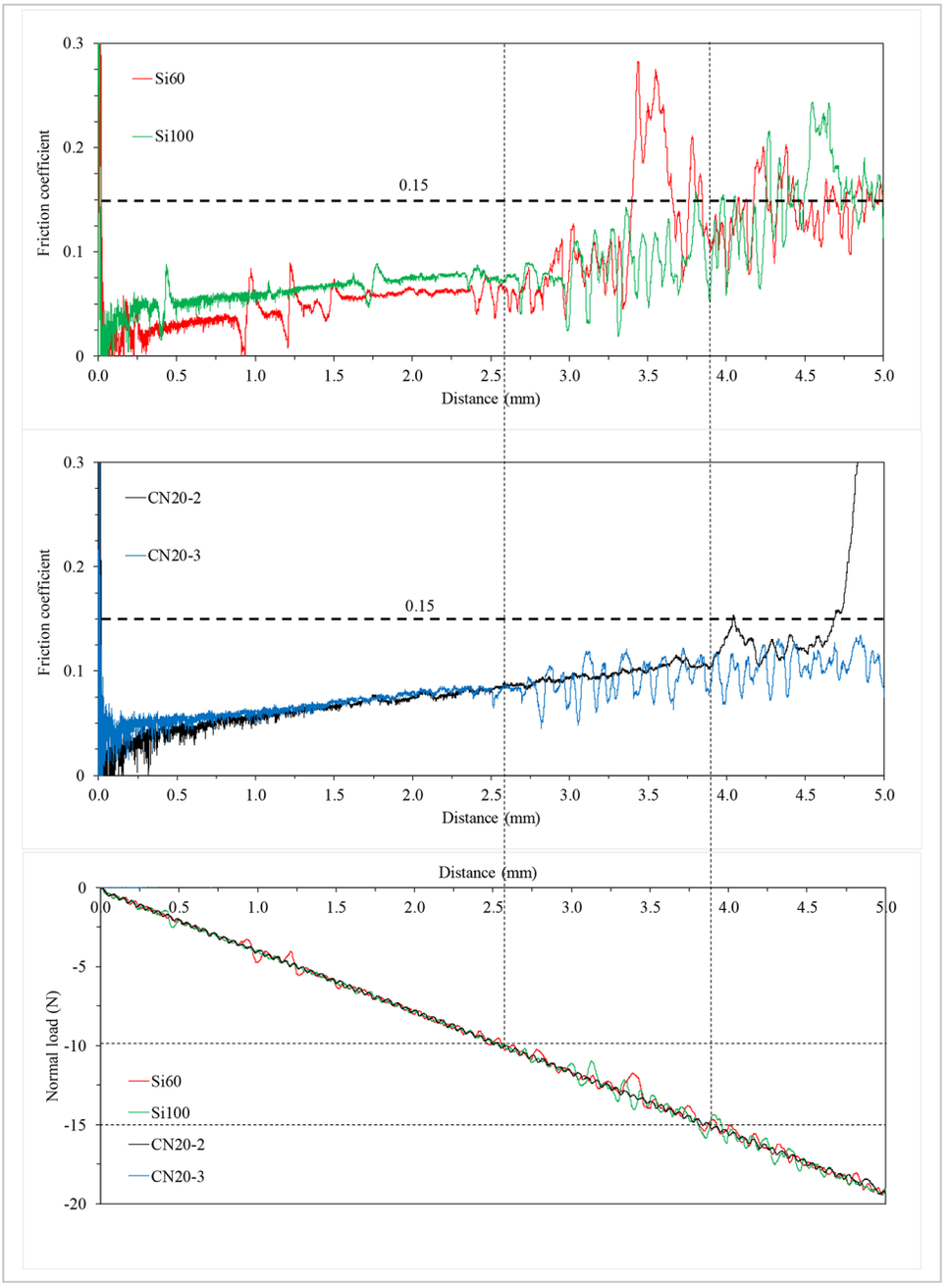

Figure 16 - Friction coefficients and normal loads of theSi60, Si100, CN20-2, and CN20-3 samples.

4. Conclusions

In this study, experiments were performed in a hollow cathode PECVD reactor aiming to compare the adhesion of DLC films grown on titanium substrates using a silicon interlayer and DLC films grown directly on carbonitrided titanium substrates. The argon flow was also changed to analyze its influence on the properties and adhesion of the DLC films. Increasing the argon flow from 20 sccm to 80 sccm in the samples with silicon interlayer increased the film hardness by more than 2,000 MPa in. The rising of the argon flow also improved the silicon interlayer adherence, observed in the VDI 3198 indentation test and promoted an increase of 41% in the film toughness. The samples where the DLC films were grown with higher process times, presented a higher adherence, due to the role of the film thickness in decreasing the influence of substrate roughness. These results confirm that the argon flow in the PECVD process can be used for tuning the hardness, adherence, and toughness of DLC films. The carbonitriding process, in turn, promoted an increase of 6.6% in the DLC film toughness and was able to maintain the friction coefficient at lower values than those obtained with the use of silicon interlayers. Considering this result and the reduced cost and easier handling of the nitrogen precursors, the carbonitriding process is more appropriate to improve the adhesion of the Ag-DLC films on Ti6Al4V alloy.

Acknowledgement

The authors acknowledge the financial support of the Brazilian Research Foundations CNPq (grant no. 560054/2010-6), CAPES, FINEP, and FAPESP (grant no. 2011/14038-4). They also thank the following institutions for use of their characterization equipments: Universidade Federal de São Paulo – UNIFESP, Instituto Tecnológico de Aeronáutica - ITA/DCTA, and Instituto de Estudos Avançados - IEAv/DCTA.

References

ALI, S.; RANI, A. M. A.; MUFTI, R. A.; HASTUTY, S.; HUSSAIN, M.; SHEHZAD, N.; BAIG, Z.; ALIYU, A. A. A. An efficient approach for nitrogen diffusion and surface nitriding of boron-titanium modified stainless steel alloy for biomedical applications. ***Metals,*** 9, p. 1-14, 2019.

AMERICAN SOCIETY FOR TESTING AND MATERIALS - ***ASTM C1624-05.*** Standard test method for adhesion strength and mechanical failure modes of ceramic coatings by quantitative single point scratch testing. ASTM, 2015.

BALACHANDRAN, S.; ZACHARIAH, Z.; FISCHER, A.; MAYWEG, D.; WIMMER, M. A.; RAABE, D.; HERBIG, M. Atomic scale origin of metal ion release from hip implant taper junctions. ***Advanced Science,*** v. 7, n. 5, p. 1-10, 2020.

BATORY, D.; JEDRZEJCZAK, A.; KACZOROWSKI, W.; SZYMANSKI, W.; KOLODZIEJCZYK, L.; CLAPA, M.; NIEDZIELSKI, P. Influence of the process parameters on the characteristics of silicon-incorporated a-C:H:SiO_x coatings. ***Surface and Coating Technology,*** v. 271, p. 112-118, 2015.

BEWILOGUA, K.; BIALUCH, I.; RUSKE, H.; WEIGEL, K. Preparation of a-C:H/a-C:H:Si:O and a-C:H/a-C:H:Si multilayer coatings by PACVD. ***Surface and Coating Technology,*** 206, p. 623-629, 2011.

BIGERELLE, M.; ANSELME, K. A kinetic approach to osteoblast adhesion on biomaterial surface. ***Journal of Biomedical Material Research.,*** v. 75A, p. 530, 2005.

BONETTI, L. F.; CAPOTE, G.; SANTOS, L. V.; CORAT, E. J.; TRAVA-AIROLDI, V. J. Adhesion studies of diamond-like carbon films deposited on Ti6Al4V substrate with a silicon interlayer. ***Thin Solid Films,*** v. 515, n. 1, p. 375-379, 2006.

BOOTKUL, D.; SUPSERMPOL, B.; SAENPHINIT, N.; ARAMWIT, C.; INTARASIRI, S. Nitrogen doping for adhesion improvement of DLC film deposited on Si substrate by Filtered Cathodic Vacuum Arc (FCVA) technique. ***Applied Surface Science,*** v. 310, n. 15, p. 284-292, 2014.

BULL, S. J.; BERASETEGUI, E. G. An overview of the potential of quantitative coating adhesion measurement by scratch testing. ***Tribology International,*** 39, p. 99-114, 2006.

BURNETT, P. J.; RICKERBY, D. S. The scratch adhesion test: an elastic-plastic indentation analysis. ***Thin Solid Films,*** 157, p. 233-254, 1988.

ÇAHA, I.; ALVES, A. C.; AFFONÇO, L. J.; LISBOA-FILHO, P. N.; DA SILVA, J. H. D.; ROCHA, L. A.; PINTO, A. M. P.; TOPTAN, F. Corrosion and tribocorrosion behaviour of titanium nitride thin films grown on titanium under different deposition times. ***Surface and Coatings Technology,*** 374, p. 878-888, 2019.

CAMPOCCIA, D.; MONTANARO, L.; ARCIOLA, C. R. A review of the biomaterials technologies for infection-resistant surfaces. ***Biomaterials,*** 34, p. 8533-8554, 2013.

CAPOTE, G.; LUGO, D. C.; GUTIÉRREZ, J. M.; MASTRAPA, G. C.; TRAVA-AIROLDI, V. J. Effect of amorphous silicon interlayer on the adherence of amorphous hydrogenated carbon coatings deposited on several metallic surfaces. ***Surface and Coatings Technology,*** 344, 644-655, 2018.

CARAVACA, F. C. ***Modified functional surfaces for increased biointegration***: surface chemistry, mechanical integrity and long-term stability of zirconia and alumina based ceramics. Tese (Doutorado) - Université de Lyon - INSA, Lyon, France, 2016. 142 f.

CEMIN, F.; BIM, L. T. MENEZES, C. M. AGUZZOLI, C.; MAIA DA COSTA, M. E. H. BAUMVOL, I. J. R.; FIGUEROA, C. A. On the hydrogenated silicon carbide (SiC_x:H) interlayer properties prompting adhesion of hydrogenated amorphous carbon (a-C:H) deposited on steel. ***Vacuum,*** 109, p. 180-183, 2014.

CHAU-CHANG, C.; YI-YANG, W.; JYH-WEI, L. JEN-CHING, H.; CHI-HSIAO, Y. Mechanical properties of fluorinated DLC and Si interlayer on a Ti biomedical alloy. ***Thin Solid Films,*** 528, p. 136-142, 2013.

CHEHUNG, W.; CHIEN-HUNG, C. The effect of thermal and plastic mismatch on stress distribution in diamond like carbon film under different interlayer/substrate system. ***Diamond and Related Materials,*** 7, v. 17, p. 1534-1540, 2008.

CHEN, M.; VON, M. A. Formation of nucleoplasmic protein aggregates impairs nuclear function in response to SiO_2 nanoparticles. ***Exp. Cell. Res.,*** 305, p. 51-62, 2005.

CHOI, H. W.; DAUSKARDT, R. H.; LEE, S. C.; LEE, K. R.; OH, K. H. CharacteristicS of silver doped DLC films on surface properties and protein adsorption. ***Diamond and Related Materials,*** v. 17, n. 3, p. 252-257, 2008.

DA SILVA, J. S. P.; RODRIGUES, A. O. N.; ALVES JR, C. Osteoblastlike cell adhesion on titanium surfaces modified by plasma nitriding. ***The International Journal of Oral & Maxillofacial Implants,*** v. 26, n. 238, 2011.

DE MORAIS, L. S.; SERRA, G. G.; ALBUQUERQUE PALERMO, E. F.; ANDRADE, L. R.; MÜLLER, C. A.; MEYERS, M. A. ELIAS, C. N. Systemic levels of metallic ions released from orthodontic mini-implants. ***American Journal of Orthodontics and Dentofacial Orthopedics,*** v. 135, n. 4, p. 522-529, 2009.

DERRADJI, N. E.; MAHDJOUBI, M. L.; BELKHIR, H.; MUMUMBILA, N.; ANGLERAUD, B.; TESSIER, P. Y. Nitrogen effect on the electrical properties of CN_x thin films deposited by reactive magnetron sputtering. ***Thin Solid Films,*** v. 482, n. 1-2, p. 258-263, 2005.

FU, Y.; DU, H.; SUN, C. Q. Interfacial structure, residual stress and adhesion of diamond coatings. ***Thin Solid Films,*** 424, p. 107-114, 2003.

FU, Y.; YAN, B. LO, N. L. Effects of pre-treatments and interlayers on the nucleation and growth of diamond coatings on titanium substrates. ***Surface and Coatings Technology,*** v. 130, n. 2-3, p. 173-185, 2000.

GAJSKI, G.; JELCČIĆ, Ž.; OREŠČANIN, V.; GERIć, M.; KOLLAR, R.; GARAJ-VRHOVAC, V. Physico-chemical characterization and the in vitro genotoxicity of medical implants metal alloy (TiAlV and CoCrMo) and polyethylene particles in human lymphocytes. ***Biochimica et Biophysica Acta (BBA)*** - General Subjects, v. 1840, n. 1, p. 565-576, 2014.

GRENADYOROV, A. S.; SOLOVYEV, A. A.; OSKOMOV, K. V.; SYPCHWENKO, V. S. Influence of deposition conditions on mechanical properties of a-C:H:SiO_x films prepared by plasma-assisted chemical vapor deposition method. ***Surface and Coatings Technology,*** 349, p. 547-555, 2018.

HAINSWORTH, S. V.; UHURE, N. J. Diamond-Like Carbon coatings for tribology: production techniques, characterization methods and applications. ***International Materials Reviews,*** v. 52, n. 3, p. 49-50, 2013.

HAUERT, R. An overview on the tribological behaviour of Diamond-Like Carbon in technical and medical applications. ***Tribology International,*** v. 11-12, n. 37, p. 991-1003, 2004.

HAUERT, R.; THORWARTH, K.; THORWARTH, G. An overview on diamond-like carbon coatings in medical applications. ***Surface & Coating Technology,*** 1, 2013, Vol. 233, pp. 119-130.

HELLMICH, A.; JUNG, T.; KIELHORN, A.; RISLAND, M. CVD-process by Hollow Cathode Glow Discharge. ***Surface and Coating Technology,*** v. 98, p. 1541-1546, 1998.

JONES, B. J.; NELSON, N. Sticking non-stick: surface and structure control of Diamond-Like Carbon in plasma enhanced chemical vapour deposition. ***Journal of Physics: Conference,*** 768, 012011, 2016.

KAEWAMATAWONG, T.; SHIMADA, A.; OKAJIMA, M.; INOUE, H.; MORITA, T.; INOUE, K.; TAKANO, H. Acute and subacute pulmonary toxicity of low dose of ultrafine colloidal silica particles in mice after intratracheal instillation. ***Toxicol Pathol,*** v. 7, n. 34, p. 958-965, 2006.

KHANDAKER, M.; RIAHINEZHAD, S.; LI, Y.; VAUGHAN, M. B.; SULTANA, F.; MORRIS, T. L.; HOSSAIN, K. Plasma nitriding of titanium alloy: effect of roughness, hardness, biocompatibility, and bonding with bone cement. ***Bio-Medical Materials and Engineering,*** v. 27, n. 5, p. 461-474, 2016.

KHETTACHE, A.; TOUHAMI, M. Z.; HEINRICH, B. H.; MAHDJOUBI, L.; BOUZABATA, B.; HORST, W. Influence of argon flow rate on the surface morphology and roughness of the DLC films prepared by MW ECR/PACVD. ***Carbon,*** C01, p. 857-858, 2002.

KIM, J.; LEE, C. Dependence of the physical properties DLC films by PECVD on the ar gas addition. Journal of the Korean Physical Society, 42, p. 956-960, 2003.

KOIKE, J.; PARKIN, D. M.; MITCHELL, T. E. Displacement threshold energy for type IIa diamond. ***Applied Physics Letters,*** v. 60, n. 12, p. 1450-1452, 1992.

LACKNER, J. M.; WALDHAUSER, W.; HARTMANN, P.; BRUCKERT, F.; WEIDENHAUPT, M.; MAJOR, R.; SANAK, M.; WIESINGER, M.; HEIM, D. Hemocompatibility of inorganic Physical Vapor Deposition (PVD) coatings on thermoplastic polyurethane polymers. ***J Funct Biomater.,*** v. 3, p. 283-297, 2012.

LIGOT, J.; BENAYOUN, S.; HANTZPERGUE, J. J. Analysis of cracking induced by scratching of tungsten coatings on polyimide substrate. ***Wear.*** v. 1-2, n. 243, p. 85, 2000.

LIMA-OLIVEIRA, D. A.; COSTA, R. P. C.; MARTINS, G. V.; CORAT, E. J.; TRAVA-AIROLDI, V. J.; LOBO, A. O.; MARCIANO, F. R. Adhesion studies of Diamond-Like Carbon films deposited on Ti6Al4V alloy after

carbonitriding. ***Open Journal of Metal,*** 2, p. 1-7, 2012.
LIN, J. F.; WEI, P. J.; PAN, J. C.; AI, C. F. Effect of nitrogen content at coating film and film thickness on nanohardness and Young's modulus of hydrogenated carbon films. ***Diamond and Related Materials,*** 13, p. 42-53, 2004.
LIN, L. H.; CHEN, S. C.; WU, C. Z.; HUNG, J. M. OU, K. L. Microstructure and antibacterial properties of microwave plasma nitrided layers on biomedical stainless steels. ***Applied Surface Science,*** v. 257, n. 17, p. 7375-7380, 2011.
LIN, W.; HUANG, Y. W.; ZHOU, X. D.; MA, Y. In vitro toxicity of silica nanoparticles in human lung cancer cells. ***Toxicol Appl Pharmacol,*** 217, p. 252-259, 2006.
LIU, X.; CHU, P. K.; DING, C. Surface modification of titanium, titanium alloys, and related materials for biomedical applications. ***Materials Science and Engineering,*** R 47, p. 49-121, 2004.
LIU, X.; CHU, P. K.; DING, C. Surface modification of titanium, titanium alloys, and related materials for biomedical applications. ***Materials Science and Engineering,*** 47, p. 103-105, 2004.
LUGO, D. C.; SILVA, P. C.; RAMIREZ, M. A.; PILLACA, E. J. D. M.; RODRIGUES, C. L.; FUKUMASU, N. K.; TRAVA-AIROLDI, V. J. Characterization and tribologic study in high vacuum of hydrogenated DLC films deposited using pulsed DC PECVD system for space applications. ***Surface and Coatings Technology,*** 332, 135-141, 2017.
LUO, D. ***Selection of coatings for tribological applications.*** Tese (Doutorado) - L'Ecole Centrale de Lyon, France, 2009.
MA, X. G.; KOMVOPOULOS, K.; WAN, D.; BOGY, D. B.; KIM, Y. S. Effects of film thickness and contact load on nanotribological properties of sputtered amorphous carbon thin films. ***Wear.*** v. 10, n. 254, p. 1010-1018, 2003.
MESKINIS, Š.; TAMULEVICIENE, A. Structure, properties and applications of diamond like nanocomposite (SiO_x Containing DLC) films: a review. ***Materials Science.*** v. 17, n. 4, 2011.
OLIVER, J. N.; SU, Y.; LU, X.; KUO, P. H.; DU, J. Bioactive glass coatings on metallic implants for biomedical applications. ***Bioactive Materials.*** v. 4, p. 261-270, 2019.
PEI, Y. T.; GALVAN, D.; DE HOSSON, J. T. M. Nanostructure and properties of TiC/a-C: H composite coatings. ***Acta Mater.,*** v. 17, n. 53, p. 4505, 2005.
PENG, X. L.; BARBER, Z. H.; CLYNE, T. W. Surface roughness of diamond-like carbon films prepared using various techniques. ***Surface and Coating Technology,*** v. 1. n. 128, p. 23-32, 2001.
PERRY, A. J. The adhesion of chemically vapour-deposited hard coatings to steel - The scratch test. ***Metallurgical and Protective Coatings.*** 78, p. 77-93, 1981.
QI, J.; CHAN, C. Y.; BELLO, I.; LEE, C. S.; LEE, S. T.; LUO, J. B.; WEN, S. Z. Film thickness effects on mechanical and tribological properties of nitrogenated diamond-like carbon films. ***Surface and Coatings Technology.*** 145, p. 38-43, 2001.
ROBERTSON, J. Diamond-like amorphous carbon. ***Materials Science and Engineering.*** 37, p. 129-281, 2002.
ROBERTSON, J. The deposition mechanism of diamond-like a-C and a-C:H. ***Diamond and Related Materials,*** 3, p. 361-368, 1994.
ROMÁN-MANSO, B.; CHEVILLOTTE, Y.; OSENDI, M. Y.; BELMONTE, M. Thermal conductivity of silicon carbide composites with highly oriented graphene nanoplatelets. ***Journal of the European Ceramic Society,*** 36, p. 3987-3993, 2016.
SAYES, C. M.; REED, K. L.; WARHEIT, D. B. Assessing toxicity of fine and nanoparticles: comparing in vitro measurements to in vivo pulmonary toxicity profiles. ***Toxicol Sci.,*** 97, p. 163-80, 2007.
SEKLER, J.; STEINEMANN, P. A.; HINTERMANN, H. E The scratch test: different critical load determination techniques. ***Surface and Coating Technology,*** 36, p. 519-529, 1988.
SHE, D.; YUE, W.; FU, Z.; WANG, C.; YANG, X.; LIU, J. Effect of nitriding temperature on microstructures and vacuum tribological properties of plasma-nitrided titanium. ***Surface and Coating Technology,*** 264, p. 32-40, 2015.
SHEEJA, D.; TAY, B. K.; LEONG, K. W.; LEE, C. H. Effect of film thickness on the stress and adhesion of diamond-like carbon coatings. ***Diamond and Related Materials,*** v. 11, p. 1643-1647, 2002.
SHUM, P. W.; LI, K. Y.; ZHOU, Z. F.; SHEN, Y. G. Structural and mechanical properties of titanium–aluminium–nitride films deposited by reactive close-field unbalanced magnetron sputtering. ***Surface and Coating Technology,*** 185, v. 2-3, 2004.
SINGH, N.; MANSHIAN, B.; JENKINS, G. J. S.; GRIFFITHS, S. M.; WILLIAMS, P. M.; MAFFEIS, T. G. G.; DOAK, S. H. NanoGenotoxicology: the DNA damaging potential of engineered nanomaterials. ***Biomaterials,*** v. 30, n. 23-24, 3891-3914, 2009.
STEFFEN, H. J.; MARTON, D.; RABALAIS, J. W. Displacement energy threshold for Ne^+ irradiation of graphite. ***Physical Review Letters,*** v. 68, n. 11, p. 1726-1729, 1992.
TOMASTIK, J.; CTVRTLIK, R.; DRAB, M.; MANAK, J. On the importance of combined scratch/acoustic emission test evaluation: SiC and SiCN thin films case study. ***Coatings,*** v. 8, n. 5, p. 196, 2018.
TAMURA, Y.; YOKOYAMA, A.; WATARI, F.; UO, M.; KAWASAKI, T. Mechanical properties of surface nitrided titanium for abrasion resistant implant materials. ***Materials Transactions,*** v. 43, n. 12, p. 3043-3051, 2002.
VALKO, M.; RHODES, C. J.; MONCOL, J.; IZAKOVIC, M.; MAZUR, M. Free radicals, metals and antioxidants in oxidative stress-induced cancer. ***Chem. Biol. Interact.,*** 160, p. 1-40, 2006.

VAN HOVE, R. P.; SIEREVELT, I. N.; VAN ROYEN, B. J.; NOLTE, P. A. Titanium-Nitride coating of orthopaedic implants: a review of the Literature. ***BioMed Research International,*** 1-9, 2015.

VANDEVELDE, T.; NESLADEK, M.; MEYKENS, K.; QUAEYHAEGENS, C.; STALS, L. M.; GOUZMAN, I.; HOFFMAN, A. On nitrogen incorporation during PE-CVD of diamonds films. ***Diamond and Related Materials,*** 7, p. 152-157, 1998.

VASUDEV, M. C.; ANDERSON, K. D.; BUNNING, T. J.; TSUKRUK, V. V. Exploration of plasma-enhanced chemical vapor deposition as a method for thin-film aabrication with biological applications. ***Appl. Mater. Interfaces,*** 5, p. 3983-3994, 2013.

VEREIN DEUTSCHER INGENIEURE NORMEN. ***Standard VDI 3198***. Dusseldorf: VDI-Verlag, 1991.

VETTER, J. 60 years of DLC coatings: historical highlights and technical review of cathodic arc processes to synthesize various DLC types, and their evolution for industrial applications. ***Surface and Coating Technology,*** 257, p. 213-240, 2014.

YONGHUI, W.; XIANG, Y. ***Exploring film failure mechanism and scratch toughness characterization of Diamond-Like Carbon film***. Cunming, China: Atlantis Press, 2015.

ZHANG, S. Titanium carbonitride-based cermets: processes and properties. ***Materials Science and Engineering,*** A163, p. 141-148, 1993.

ZHANG, S.; SUN, D.; FU, Y. Q.; DU, H.; ZHANG, Q. Effect of sputtering target power on preferred orientation in nc-TiN/a-SiN_x nanocomposite thin films. ***Journal of Metastable and Nanocrystalline Materials,*** 23, p. 175-178, 2005.

ZHANG, S.; ZHANG, X. M. Toughness evaluation of hard coatings and Thin Film. ***Thin Solid Film,*** 7, p. 2375-2389, 2012.

ZIA, A. W.; BIRKETT, M. Deposition of diamond-like carbon coatings: conventional to non-conventional approaches for emerging markets. ***Ceramics International,*** v. 47, n. 20, 28075-28085, 2021.

Received: 24 January 2024 - Accepted: 27 March 2024.